2024 IEEE/RSJ International Conference on Intelligent Robots and Systems (IROS)
October 14-18, 2024. Abu Dhabi, UAE

Segmented Safety Docking Control for Mobile Self-Reconfigurable Robots

Zhi Zheng, Tao Jiang, Senqi Tan, Hao Zhang, and Jianchuan Ye

***Abstract*—Mobile self-reconfigurable robots (MSRRs), as a novel multi-robot system with flexible configurations and task adaptability, hold promising applications in unstructured task environments. However, existing autonomous docking strategies are primarily applied in laboratory settings and face numerous challenges and limitations in actual applications, including differences in sensor characteristics, safety threats, and saturation constraints. To address these issues, this paper proposes a segmented secure docking control framework based on global localization and local perception to achieve stable and reliable reconfiguration of MSRRs in practical applications. Specific contributions include the implementation of a dual-layer constraint framework for safeness of units in the long-distance phase against velocity and acceleration nested windups, and the integration of active line-of-sight (LOS) correction and adaptive windup driving mobile units to achieve precise and rapid locking of docked positions within the LOS in the close-range phase. Finally, the validity of the proposed method is verified via physical experiments, offering an innovative approach to deploying MSRRs in complex scenarios.**

I. Introduction

Mobile self-reconfiguring robots (MSRRs), composed of multiple modules, each capable of autonomous movement and task execution, can autonomously connect via physical docking mechanisms to form flexible configurations suited for various terrains and tasks. Unlike traditional fixed-configuration robots, MSRRs offer enhanced morphological flexibility and task adaptability, showing significant promise in unstructured task environments. Consequently, the design and motion control of various mobile self-reconfiguring robot systems, such as SMORES-EP [1], MIRRAX [2], hTetro [3], STORM [4], R-track [5], and SambotII [7], have been the focus of extensive research in recent years. Efficient and precise autonomous docking of individual modules is critical to the robots' ability to adapt to different terrains and complex tasks.

Current methods of autonomous docking for MSRRs mainly operate within controlled lab environments, leveraging either local or global sensing mechanisms for unit localization and reconfiguration. In [6], infrared transceivers on MSRR units have been used to gather lateral distance information from adjacent units, facilitating the adjustment of distance errors and the issuance of speed commands for reconfiguration purposes. In [7], vision and laser sensors have been integrated to perceive the immediate surroundings, leading to the development of a three-phase combination strategy comprising wandering, pose adjustment, and docking for seamless multi-robot reconfiguration. In [8], a combination of visual and infrared sensing has been applied to design a three-phase docking strategy, enabling self-reconfiguration of robot systems through far, mid, and close phases. The employment of vision and sonar for perception has utilized neural networks in designing a docking process, including search, avoidance, and self-alignment, triggering the behavioural decisions of robot units in [9]. A three-phase docking strategy based on local infrared perception and a two-phase trajectory planning strategy involving long-distance point assembly and close-range linear guidance, under the assumption of high-precision global positioning, have been proposed to enhance the docking of dual units in [10], [11]. A kinematic error feedback control framework under the global frame has been used to devise a three-phase docking strategy of navigation, pose adjustment, and trajectory replanning for local obstacle avoidance during the navigation phase in [12]. Segmented behavioural strategies are commonly adopted in current reconfiguration docking methods to search for and perceive targets, thereby improving docking success rates. This segmented approach is similarly employed in other docking scenarios, such as carrier recovery [18] and spacecraft rendezvous [14], to enhance task efficiency.

Existing docking methods predominantly cater to simple laboratory settings and environments, relying on onboard sensors (such as vision and infrared sensors) for local perception or external vision for the high-precision global location to gather information about units and the environment. These methods achieve efficient system reconfiguration by refining target search and behaviour control. However, from the application viewpoint, networked multi-unit docking significantly benefits from the combination of long-distance proper-precision global location (e.g., satellite positioning) and close-range high-precision sensor recognition (e.g., vision) for environmental perception, aptly suiting real-world complexities.

This work was supported in part by China Postdoctoral Science Foundation under Grant 2023M731913, and in part by National Natural Science Foundation of China under Grant 62106027,52202512, and in part by Graduate Research and Innovation Foundation of Chongqing, China under Grant CYB22066, CYB23053. (*Correspongding author: Tao Jiang*.)

Z. Zheng, T. Jiang, and H. Zhang are with the School of Automation, Chongqing University, China (e-mail: zhizheng@cqu.edu.cn; jiangtao_1992@cqu.edu.cn; zhang_hao@cqu.edu.cn).

S. Tan is with China North Artificial Intelligence & Innovation Research Institute, and Collective Intelligence & Collaboration Laboratory, Senior Engineer (e-mail: tristantsq@gmail.com).

J. Ye is with Department of Computer Science and Technology, Tsinghua University, Beijing, 100084, China (e-mail: yejianchuan@yeah.net).

Hence, at the beginning of the task, global location is used to navigate the unit to the vicinity of the docked unit. Then, local perception is employed to finish the nearby docking of multiple units. Moreover, current docking control methods primarily utilize open-loop or simplistic closed-loop approaches without deeply addressing factors such as line-of-sight (LOS) constraints, environmental obstacles, and input saturation that critically affect mobile self-reconfiguring robots' safety, smoothness, and stability.

Based on analyses of the applicability and restrictions of existing methods in MSRRs, this paper proposes a segmented safety docking control framework against the input windup, LOS safety, and obstacles, achieving smooth and reliable multi-unit docking. The main contributions are as follows

1) A segmented docking control strategy based on global positioning and local perception for long-distance safe assembly and close-range guidance docking is proposed and validated via experiments for its effectiveness.
2) The novel cascading control with upper-level obstacle avoidance guidance with lower-level trajectory tracking is designed in the long-distance phase, introducing dual-layer safety constraints and an adaptive anti-windup to ensure the safeness and smoothness of assembly.
3) The new linear and nonlinear composite anti-windup controller is proposed in the close-range phase, integrating LOS safety-related expected trajectory correction to ensure rapid and smooth docking within the LOS range.

II. Robot System and Docking Strategy Design

A. Mobile Self-Reconfiguring Robot System

As illustrated in Fig. 1, the MSRR consists of multiple differential-drive wheeled mobile units. The motion control system of each unit is composed of torque motors, WiFi devices, and an integrated main control board. The docking mechanism is formed by location holes and embedded cam-locking devices. When the locking device is inserted into the location hole, it is tightened by the servo motor, enabling the reconfiguration and combination of multiple units.

B. Segmented Fault-Tolerant Reconfiguration Docking Strategy Design

Considering the limitations of real-world open scenarios and other engineering docking scenarios, the segmented docking process shown in Fig. 2 is adopted. In complex engineering scenarios, the MSRR system during the long-distance phase of segmented docking is highly likely to encounter obstacles during assembly. Considering the presence of control input windup, controller design must involve adaptive anti-windup and smooth reactive avoidance to ensure assembly safety. In the close-range phase, due to global location errors such as satellite location or indoor mapping, units assembled relative to the docked target will inevitably have a position deviation, easily triggering subsequent control input saturation and trajectory oscillation in the close-range phase. Additionally, the convergence speed and accuracy of the tracking trajectory in the phase significantly restrict whether the MSRR unit can smoothly move the locking device into the location hole. Therefore, the close-range controller design needs to integrate rapid convergence, adaptive anti-windup, and sensor LOS safety maintenance to achieve smooth docking guidance motion within the perception range. In case of docking failure, the unit will retreat along the target line and re-enter the close-range docking guidance control phase to ensure complete reconfiguration.

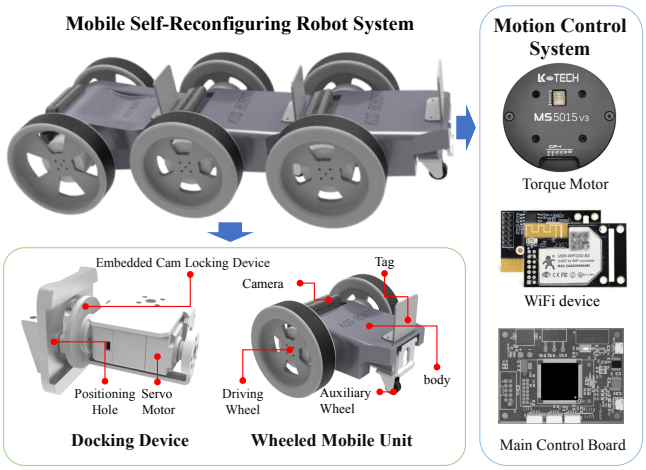

Fig. 1: Mobile Self-Reconfiguring Robot System

C. Robot Motion Model and Control Objective

The nonholonomic kinematic model of each MSRR unit [15] is written as follows

$$\begin{aligned} \dot{x}_l &= v\cos(\theta) - lw\sin(\theta), \\ \dot{y}_l &= v\sin(\theta) + lw\cos(\theta), \\ \dot{\theta}_l &= w, \end{aligned} \tag{1}$$

$$\begin{aligned} x_l &= x + l\cos(\theta), \\ y_l &= y + l\sin(\theta), \\ \theta_l &= \theta, \end{aligned} \tag{2}$$

where v and w are the linear and angular velocities of the MSRR unit, respectively, while x, y, and θ represent the unit's position and orientation in the inertial frame; l is the axial offset between the observation point and the center point. x_l, y_l, and θ_l denote the position and orientation of the unit's measurement point. The position and velocity vectors can be represented as $p_1 = [x_l, y_l]^{\mathrm{T}}$ and $p_2 = [\dot{x}_l, \dot{y}_l]^{\mathrm{T}}$.

The control inputs are linear and angular velocities. Nevertheless, in applications, Considering engineering constraints such as actuator physical limits and manoeuvre safety, amplitude and rate windup constraints should be imposed on the linear and angular velocities of each MSRR unit. The composite windup constraint model [16] is as follows

$$\begin{aligned} \dot{v}_s &= \mathrm{sat}\left(-\bar{a}, \mathrm{sat}\left(-\bar{v}, v_d, \bar{v}\right) - v_s, \bar{a}\right), \\ \dot{w}_s &= \mathrm{sat}\left(-\bar{\omega}, \mathrm{sat}\left(-\bar{w}, w_d, \bar{w}\right) - w_s, \bar{\omega}\right), \end{aligned} \tag{3}$$

where $\bar{v}$ and $\bar{a}$ represent the linear velocity and linear acceleration windups, respectively, while $\bar{w}$ and $\bar{\omega}$ denote the angular velocity and angular acceleration windups. $\dot{v}_s$ and $\dot{w}_s$ are

the saturated linear and angular velocities under the nested windup constraints. When the velocity and acceleration of the MSRR unit trigger saturation windup, it can induce severe trajectory oscillations, thereby affecting the control's smoothness and stability margin. The paper aims to achieve

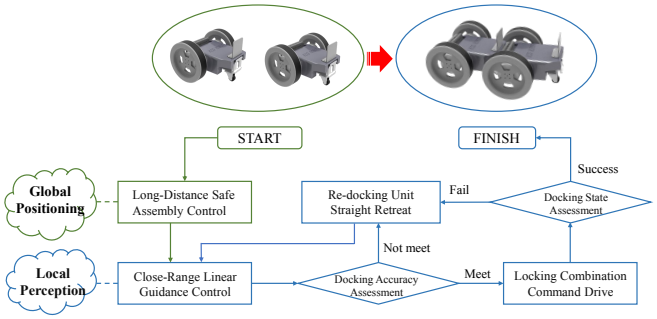

Fig. 2: Segmented Fault-Tolerant Docking Strategy

safe and smooth segmented docking control against nested windups, obstacles, and LOS safety. The critical responses for the long-distance and close-range phase tasks are as follows

1) The desired trajectory for the long-distance phase assembly can be obtained via various trajectory generation methods, where the desired trajectories x_d and y_d and their first and second derivatives are bounded. Mobile units on the desired trajectory are set to collide with obstacles (x_o, y_o). The long-distance controller is designed to achieve position tracking of the assembly trajectory, safely moving to the final assembly point.
2) For the close-range phase, the docking target installation position is considered the inertial frame to simplify the controller design, with the linear guidance trajectory represented as $x_r = f_{docking}(t), y_r = 0$. The first and second derivatives of $f_{docking}(t)$ are bounded. In application, $f_docking\,(t)$ can be provided by a trajectory generation method. The close-range controller is designed to rapidly converge within the LOS range to the guidance trajectory, ensuring the locking device is smoothly inserted into the location hole.

Lemma 1: There exists a double integrator system, barrier function, safety acceleration envelope, and control law as follows

$$\dot{\eta}_1 = \eta_2, \quad \dot{\eta}_2 = u, \tag{4}$$

$$\mathcal{B}(\eta_1, \eta_2) = \eta_2 - \mathcal{F}(\eta_1), \tag{5}$$

$$u_s(\eta_1, \eta_2) = -\alpha \mathcal{B}(\eta_1, \eta_2) + \mathcal{H}(\eta_1)\eta_2,$$

$$u = \text{sat}\left(-\bar{u}, \min\left\{u_r(\eta, \eta_r), u_s(\eta_1, \eta_2)\right\}, \bar{u}\right), \tag{6}$$

with

$$h(x) = \begin{cases} 1, & x \geq 0 \\ 0, & x < 0 \end{cases}$$

$$\beta(x) = \left[2\gamma\rho \ln\left(\cosh\left(\frac{x}{\rho}\right)\right)\right]^{\frac{1}{2}}, \quad x \leq 0$$

$$\mathcal{H}(x) = h(-x)\frac{\gamma \tanh\left(\frac{x}{\rho}\right)}{\beta(x)}\sqrt{\frac{\gamma}{\rho}}$$

$$\mathcal{F}(x) = -h(-x)\beta(x) + (1 - h(-x))\sqrt{\frac{\gamma}{\rho}}x$$

where design gains γ, ρ, and α to satisfy $0 < \gamma < \bar{u}$, $\rho > 0$, and $\alpha > 0$. The control law to be designed, $u_r(\eta, \eta_r)$, under the safety acceleration envelope (5), generates the actual control law (6), ensuring the system state η_1 always remains within the safety boundaries without disturbances [17].

Lemma 2: Consider the disturbed time-varying system as follows

$$\dot{\xi}(t) = \frac{1}{\epsilon}\mathcal{K}(t)\xi(t) + \delta(t), t \geq t_0, t_0 \in \mathbb{R}_+ \tag{7}$$

where $\mathcal{K} \in \mathcal{C}(\mathbb{R}_{\geq t_0})$, $\delta(t)$ is the disturbance term, and the initial condition $\xi(t_0)$ belongs to a compact subset of $\mathbb{R}$. Assuming the linear time-varying system $\dot{\xi}_0(t) = \mathcal{M}(t)\xi_0(t)$ is uniformly exponentially stable, and $|\delta(t)| \leq \bar{\delta}/(\varepsilon^m)$, where $\bar{\delta}$ is a positive constant independent of ε, and $m \geq 0$ is an integer. Then, for any $\sigma > 0$ and $T > 0$, there exists $\varepsilon_0 > 0$ such that for any $\varepsilon \in (0, \varepsilon_0)$ and $t \in [t_0 + T, \infty)$, the solution of equation (7) satisfies $\|\xi(t)\| \leq \sigma\varepsilon^m$ [18].

III. Long-Distance Safe Assembly Control against Nested Windups

The two-layer safety control framework with an upper-level obstacle avoidance guidance module based on the holonomic kinematic model and a lower-level adaptive anti-windup tracking module based on the nonholonomic model in Fig. 3.

A. Upper-level Obstacle Avoidance Guidance Module

For the design simplicity and task feasibility, the upper-level guidance module adopts the virtual holonomic kinematics [22] as follows

$$\dot{\varphi}_1 = \varphi_2, \quad \dot{\varphi}_2 = u^{\varphi} \tag{8}$$

where $\varphi_1 = [x^{\varphi}, y^{\varphi}]^{\mathrm{T}} \in \mathbb{R}^2$ and $\varphi_2 = \left[v_x^{\varphi}, v_y^{\varphi}\right]^{\mathrm{T}} \in \mathbb{R}^2$ represent the position and velocity states of the virtual kinematics, respectively. $u^{\varphi} = \left[a_x^{\varphi}, a_y^{\varphi}\right]^{\mathrm{T}} \in \mathbb{R}^2$ is the control input to be designed, acting as an equivalent to acceleration. The initial values satisfy $\varphi_i(0) = p_i(0)$. x^{φ}, y^{φ}, v_x^{φ}, v_y^{φ}, a_x^{φ}, and a_y^{φ} are the longitudinal and lateral position, velocity, and acceleration of the virtual kinematics in the inertial frame.

The longitudinal and lateral safety acceleration envelopes near obstacles during the long-range docking phase are designed as follows

$$\begin{aligned} a_{xs}^{\varphi t} &= -\alpha \mathcal{B}(\bar{x}_t^{\varphi}, \dot{\bar{x}}_t^{\varphi}) + \mathcal{H}(\bar{x}_t^{\varphi})\dot{\bar{x}}_t^{\varphi} \\ a_{ys}^{\varphi t} &= -\alpha \mathcal{B}(\bar{y}_t^{\varphi}, \dot{\bar{y}}_t^{\varphi}) + \mathcal{H}(\bar{y}_t^{\varphi})\dot{\bar{y}}_t^{\varphi}, \quad t = u, l \end{aligned} \tag{9}$$

where $\bar{x}_u^{\varphi} = x^{\varphi} - x_o^u$, $\bar{x}_l^{\varphi} = x_o^l - x^{\varphi}$, $\bar{y}_u^{\varphi} = y^{\varphi} - y_o^u$, and $\bar{y}_l^{\varphi} = y_o^l - y^{\varphi}$; x_o^u, x_o^l, y_o^u, and y_o^l are the safety walls set according to the obstacle position, (x_o, y_o).

The acceleration envelope constraint also triggers saturation oscillations. Introduce the adaptive auxiliary dynamic system to smooth the virtual trajectory as follows

$$\begin{aligned} \dot{\lambda}_x^{\varphi} &= \cosh^2(\lambda_x^{\varphi})\left(-k_x^{\varphi}\lambda_x^{\varphi} + \Delta_x^{\varphi}\right)/\gamma^{\varphi}, \\ \dot{\lambda}_y^{\varphi} &= \cosh^2\left(\lambda_y^{\varphi}\right)\left(-k_y^{\varphi}\lambda_y^{\varphi} + \Delta_y^{\varphi}\right)/\gamma^{\varphi}, \end{aligned} \tag{10}$$

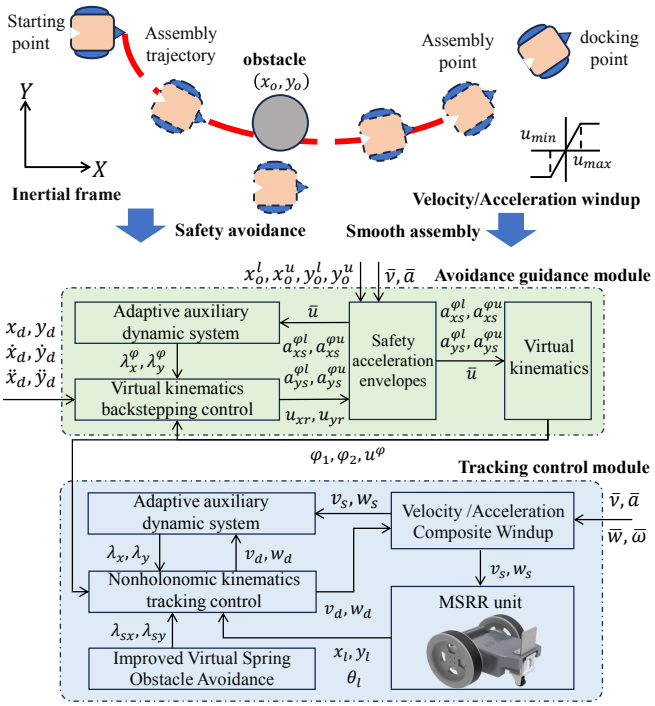

Fig. 3: Guidance-Tracking Dual-Layer Safety Control Framework

where λ_x^φ and λ_y^φ are the auxiliary dynamic variables in the longitudinal and lateral directions; k_x^φ, k_y^φ, $\gamma^\varphi \in \mathbb{R}_+$ are the designed positive gains; u_{xr} and u_{yr} are the longitudinal and lateral control laws to be designed; the deviation between the virtual dynamic acceleration windups and the longitudinal/lateral control inputs are $\Delta_x^\varphi = u_{xs} - u_{xr}$ and $\Delta_x^\varphi = u_{ys} - u_{yr}$, with $a_x^\varphi = \text{sat}\left(-\bar{u}, \text{sat}\left(-a_{xs}^{\varphi l}, u_{xr}, a_{xs}^{\varphi u}\right), \bar{u}\right)$ and $a_y^\varphi = \text{sat}\left(-\bar{u}, \text{sat}\left(-a_{ys}^{\varphi l}, u_{yr}, a_{ys}^{\varphi u}\right), \bar{u}\right)$ being the control inputs after the safety acceleration envelope constraints. According to Lemma 1, the trajectory of the constrained virtual dynamic system can be ensured to move within the specified safety region, avoiding collisions.

Design the longitudinal and lateral control inputs through backstepping as follows

$$\begin{aligned} u_{rx} &= -c_2 z_{2x} + \ddot{x}_d - k_x^\varphi \lambda_x^\varphi - z_{1x} - c_1 \left(z_{2x} + c_1 z_{1x}\right), \\ u_{ry} &= -c_2 z_{2y} + \ddot{y}_d - k_y^\varphi \lambda_y^\varphi - z_{1y} - c_1 \left(z_{2y} + c_1 z_{1y}\right) \end{aligned} \tag{11}$$

where $z_{1x} = x^\varphi - x_d$ and $z_{1y} = y^\varphi - y_d$ are position tracking errors; $v_{xr}^\varphi = \dot{x}_d - c_1 z_{1x}$ and $v_{yr}^\varphi = \dot{y}_d - c_1 z_{1y}$ are virtual commands; $z_{2x} = v_x^\varphi - v_{xr}^\varphi - \gamma_x^\varphi \tanh\left(\lambda_x^\varphi\right)$ and $z_{2y} = v_y^\varphi - v_{yr}^\varphi - \gamma_y^\varphi \tanh\left(\lambda_y^\varphi\right)$ are velocity tracking errors; c_1 and c_2 are positive control gains.

The Lyapunov function is written as follows

$$V_u = \frac{1}{2} z_{1x}^2 + \frac{1}{2} z_{2x}^2 + \frac{1}{2} z_{1y}^2 + \frac{1}{2} z_{2y}^2. \tag{12}$$

Taking the derivative of it yields

$$\dot{V}_u \leq -c V_u, \tag{13}$$

where $c = 0.5 \min\{c_1, c_2\} > 0$. The integrals and their double integrals of u_{xr} and u_{yr} are $\dot{x}_{rl}$, $\dot{y}_{rl}$, x_{rl}, and y_{rl}, and the signals generated from them serve as the desired signals for the lower-level trajectory tracking. Therefore, only the lower-level actual trajectory can precisely track the generated guidance trajectory, and the upper-level control system will be stable.

B. Lower-level Adaptive Anti-windup Tracking Module

The generated trajectory tracking control scheme with adaptive anti-windup and virtual spring obstacle avoidance strategies is designed to finish the dual-layer constraint mechanism with upper-level guidance.

Combining the kinematics (1) and the nested windup model (3), the adaptive anti-windup is designed as follows

$$\begin{aligned} \dot{\lambda}_x &= \cosh^2\left(\lambda_x\right)\left(-k_x \lambda_x + \Delta_x\right)/\gamma_x, \\ \dot{\lambda}_y &= \cosh^2\left(\lambda_y\right)\left(-k_y \lambda_y + \Delta_y\right)/\gamma_y, \end{aligned} \tag{14}$$

wherein the deviation between the saturated velocity and velocity command is allocated in the motion space as follows

$$\begin{aligned} \Delta_x &= (v_s - v)\cos(\theta) - l(w_s - w)\sin(\theta), \\ \Delta_y &= (v_s - v)\sin(\theta) + l(w_s - w)\cos(\theta), \end{aligned}$$

λ_x and λ_y are auxiliary dynamic variables in the longitudinal and lateral directions; k_x, k_y, γ_x, and γ_y are positive adaptive gains.

The repulsive force exerted by the obstacle, (x_o, y_o), on the MSRR unit mimicking the action of a spring is represented as

$$F_{ro} = \begin{cases} k_r \tanh\left(\tan\left(\frac{\pi}{2}\frac{\rho_{sR} - \rho_{ro}}{\rho_{sR} - \rho_{sr}}\right)\right), & \rho_{ro} \leq \rho_{sR} \\ 0, & \rho_{ro} > \rho_{sR} \end{cases}, \tag{15}$$

where $\rho_{ro} = \| [x_l, y_l]^{\mathrm{T}} - [x_o, y_o]^{\mathrm{T}} \|$ represents the distance between the robot and the obstacle, ρ_{sr} and ρ_{sR} denote the upper and lower bounds of the collision avoidance distance, and k_r is the spring constant. The design and parameter selection of $k_r \tanh(\cdot)$ are related to the boundedness of energy and the windup of acceleration. The entire repulsive force function reflects the closed-loop dynamic adjustment mechanism of the robot's distance from the obstacle. Similarly, embedding an auxiliary dynamic system into the controller ensures the system's safety performance. The specific design is as follows

$$\begin{aligned} \dot{\lambda}_{sx} &= \cosh^2\left(\lambda_{sx}\right)\left(-k_{sx}\lambda_x + \Delta_{sx}\right)/\gamma_{sx}, \\ \dot{\lambda}_{sy} &= \cosh^2\left(\lambda_{sy}\right)\left(-k_{sy}\lambda_y + \Delta_{sy}\right)/\gamma_{sy}, \end{aligned} \tag{16}$$

where λ_{sx} and λ_{sy} are auxiliary dynamic variables for velocity correction, k_{sx}, k_{sy}, γ_{sx}, and γ_{sy} are positive adaptive gains; $\Delta_{sx} = F_{ro}\cos\left(\theta_{ro}\right)$, $\Delta_{sy} = F_{ro}\sin\left(\theta_{ro}\right)$, and θ_{ro} is the angle between the repulsion LOS and the unit axis in its frame.

Combining the control model (1), the adaptive anti-windup strategy (14), and the lower-level obstacle avoidance (15) and

(16), the lower-level tracking errors e_{xl}, e_{yl}, and control laws u_{xd}, u_{yd} are designed as follows

$$\begin{aligned} e_{xl} &= x_l - x_{rl} - \gamma_x \tanh(\lambda_x), \\ e_{yl} &= y_l - y_{rl} - \gamma_y \tanh(\lambda_y), \end{aligned} \tag{17}$$

$$\begin{aligned} u_{xd} &= -k_{xl} e_{xl} + \dot{x}_{rl} - k_x \lambda_x - \gamma_{sx} \tanh(\lambda_{sx}), \\ u_{yd} &= -k_{yl} e_{yl} + \dot{y}_{rl} - k_y \lambda_y - \gamma_{sy} \tanh(\lambda_{sy}), \end{aligned} \tag{18}$$

where $k_{xl} > 0$ and $k_{yl} > 0$ represent the control gains. Through the matching mapping relationship in (1) between linear/angular velocities and longitudinal/lateral velocities, the linear/angular velocities v and w can be obtained.

To demonstrate the stability of the bottom tracking module, the following Lyapunov function is designed as

$$V_l = \frac{1}{2} e_{xl}^2 + \frac{1}{2} e_{yl}^2, \tag{19}$$

and its derivative is deduced as follows

$$\dot{V}_l \leq -c_{xl} e_{xl}^2 - c_{yl} e_{yl}^2 + \Delta_S, \tag{20}$$

Where $\Delta_S > \gamma_{sx}^2 \tanh^2(\lambda_{sx}) + \gamma_{sy}^2 \tanh^2(\lambda_{sy}) > 0$, $c_{xl} = k_{xl} - 0.25 > 0$, $c_{yl} = k_{yl} - 0.25 > 0$, and $k_{xl} > 0.25$, $k_{yl} > 0.25$.

Combining these, we have $\dot{V}_l = -c_l V_l + \Delta_S$, where $c_l = 0.5 \min\{c_{xl}, c_{yl}\}$. According to Lemma 2, Δ_S is bounded and rapidly decays after collision avoidance. Hence, the lower-level tracking control module is stable, and the range of tracking errors e_{xl} and e_{yl} can be adjusted via control gains.

IV. Close-range Fast Docking Control within the LOS Constraint

The rapid-convergence linear/nonlinear composite controller framework, integrating adaptive anti-windup and active trajectory correction based on the LOS cone safety, is in Fig. 4.

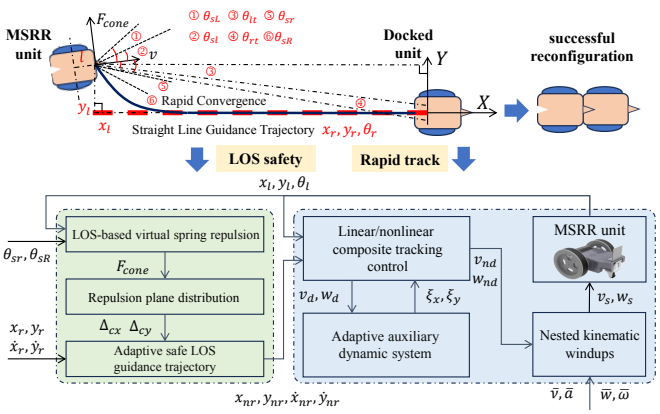

Fig. 4: Rapid Convergence Control Framework within Safety LOS

A. Adaptive Compensation for Guidance Trajectory Based on LOS Cone

LOS constraints and environmental obstacles are similar in that they are crucial safety metrics that cannot be overlooked during the control process. In the kinematic layer, close-range docking control employs the same kinematic control framework as the remote assembly stage, designing longitudinal and lateral motion commands. These commands are converted into linear and angular velocities through velocity distribution but do not directly involve posture adjustments to meet the safety requirements of LOS constraints. Therefore, an adaptive compensation item for the desired trajectory is designed based on the LOS cone that maintains perceptual safety. This online adjusts the desired trajectory to ensure that the docked target always remains within the robot's perceptual LOS range.

The concept of adaptive compensatory design for the desired trajectory is similar to the approach used in [19], who adjusted the desired trajectory using an Artificial Potential Field (APF), but considering the APF's intense reaction as the robot approaches the LOS cone, it is easy to trigger windup. Consequently, this can fail to ensure the safety of maintaining LOS in actual experiments. Therefore, this section adopts the spring obstacle avoidance strategy described in the previous section to design the adaptive compensation items Δ_{x_r} and Δ_{y_r}, and the new reference trajectory is written as follows

$$x_{nr} = x_r + \Delta_{x_r}, y_{nr} = \Delta_{y_r}, \tag{21}$$

The repulsive force clusters at the measured position of the MSRR units within and outside the boundary of the LOS cone can be represented as

$$\begin{aligned} F_{cone}^{lR} &= \begin{cases} k_{cone} \tanh\left(\tan\left(\frac{\pi}{2} \frac{\theta_{sR} - \theta_{lt}}{\theta_{sR} - \theta_{sr}}\right)\right), & \theta_{lt} \geq \theta_{sr} \\ 0, & \theta_{lt} < \theta_{sr} \end{cases}, \\ F_{cone}^{rR} &= \begin{cases} k_{cone} \tanh\left(\tan\left(\frac{\pi}{2} \frac{\theta_{sR} - \theta_{rt}}{\theta_{sR} - \theta_{sr}}\right)\right), & \theta_{rt} \geq \theta_{sR} \\ 0, & \theta_{rt} < \theta_{sR} \end{cases}, \\ F_{cone}^{lL} &= \begin{cases} k_{cone} \tanh\left(\tan\left(\frac{\pi}{2} \frac{\theta_{sL} - \theta_{lt}}{\theta_{sL} - \theta_{sl}}\right)\right), & \theta_{lt} \geq \theta_{sL} \\ 0, & \theta_{lt} < \theta_{sL} \end{cases}, \\ F_{cone}^{rL} &= \begin{cases} k_{cone} \tanh\left(\tan\left(\frac{\pi}{2} \frac{\theta_{sL} - \theta_{rt}}{\theta_{sL} - \theta_{sl}}\right)\right), & \theta_{rt} \geq \theta_{sR} \\ 0, & \theta_{rt} < \theta_{sR} \end{cases}, \end{aligned} \tag{22}$$

where $k_{cone} > 0$ is the elastic coefficient, θ_{sl}, θ_{sL}, θ_{sr}, and θ_{sR} are the inner and outer safety boundaries of the left and right sides of the LOS cone; θ_{lt} and θ_{rt} are the angles of the line of sight on the left and right sides of the target, relative to the robot's frame. When θ_{lt} or θ_{rt} starts to enter the range $[\theta_{sl}, \theta_{sL}]$ or $[\theta_{sr}, \theta_{sR}]$ the repulsive force begins to act, forcing the robot's line of sight angles on both sides to re-enter the safe range $[\theta_{sl}, \theta_{sr}]$.

Introducing torque to stimulate adjustments in the reference trajectory through the force distribution method, the re-

pulsive forces for longitudinal and lateral actions are designed as

$$\Delta_{cx} = \left(F_{cone}^{lR} + F_{cone}^{lL}\right)\cos\theta_{lt} + \left(F_{cone}^{rR} + F_{cone}^{rL}\right)\cos\theta_{rt},$$
$$\Delta_{cy} = \left(F_{cone}^{lR} + F_{cone}^{lL}\right)\sin\theta_{lt} + \left(F_{cone}^{rR} + F_{cone}^{rL}\right)\sin\theta_{rt}, \quad (23)$$

where Δ_{cx} is the longitudinal repulsive force, and Δ_{cy} is the lateral repulsive force.

Through the auxiliary dynamic system, adaptive compensation items are generated to correct the reference trajectory, thereby creating new safe guidance trajectories, as follows

$$\dot{\lambda}_{1cx} = -k_{1cx}\lambda_{1cx} + \lambda_{2cx}, \dot{\lambda}_{2cx} = -k_{2cx}\lambda_{2cx} + \Delta_{cx},$$
$$\dot{\lambda}_{1cy} = -k_{1cx}\lambda_{1cy} + \lambda_{2cy}, \dot{\lambda}_{2cx} = -k_{2cy}\lambda_{2y} + \Delta_{cy}, \quad (24)$$

where k_{1cx}, k_{2cx}, k_{1cy}, and k_{2cy} are positive adaptive gains, and λ_{1cx}, λ_{2cx}, λ_{1cy}, and λ_{2cy} are adaptive auxiliary signals. λ_{1cx} and λ_{1cy} serve as pose correction signals, boundedness and convergence similar to the previous section can be derived from Lemma 2, thus the adaptive compensation terms are designed as $\Delta_{x_r} = \lambda_{1cx}$ and $\Delta_{y_r} = \lambda_{1cy}$.

B. Linear and Nonlinear Composite Tracking Controller

The rapid tracking of the guidance trajectory by the tracking controller designed in the close-range docking phase is a prerequisite for reliable docking. Inspired by the linear and nonlinear composite control methods in [20] and predefined-time convergence in [21] based segmented nonlinear feedback to improve the convergence speed of the system during transient processes, a composite linear/nonlinear control term for rapid transient convergence is introduced in the close-range phase. This approach achieves fast convergence to the straight-line guidance trajectory, ensuring that the locking device smoothly enters the location hole over short distances. Additionally, for the convenience of controller design, a coordinate transformation is employed, considering the stationary position of the docked target as the new inertial frame to represent the position and orientation of the moving unit.

The adaptive anti-windup design for the close-range stage is similar to that for the long-distance assembly stage, and it is written as follows

$$\dot{\xi}_x = \cosh^2(\xi_x)\left(-k_x\xi_x + \Delta_x\right)/\gamma_x,$$
$$\dot{\xi}_y = \cosh^2(\xi_y)\left(-k_y\xi_y + \Delta_y\right)/\gamma_y, \quad (25)$$

where ξ_x and ξ_y are auxiliary dynamic variables, k_x, k_y, γ_x, and γ_y are positive tuning gains.

The tracking errors and linear/nonlinear composite control terms are designed as follows

$$\begin{aligned} e_{nx} &= x_n - x_{nr} - \gamma_x \tanh(\xi_x), \\ e_{ny} &= y_n - y_{nr} - \gamma_y \tanh(\xi_y), \end{aligned} \quad (26)$$

$$\begin{aligned} u_{xr} &= -k_{nx}e_{nx} - \frac{e^{|e_{nx}|^{-\alpha_x}}\,\mathrm{sig}(e_{nx})^{1-\alpha_x}}{\alpha_x T_x} + \dot{x}_{nr} - k_x\xi_x, \\ u_{yr} &= -k_{ny}e_{ny} - \frac{e^{|e_{ny}|^{-\alpha_y}}\,\mathrm{sig}(e_{ny})^{1-\alpha_y}}{\alpha_y T_y} + \dot{y}_{nr} - k_y\xi_y, \end{aligned} \quad (27)$$

where x_n and y_n represent the position of the mobile unit in the docked target frame, $k_{nx} > 0$ and $k_{ny} > 0$ are linear control gains, and $0 < \alpha_x < 1$, $0 < \alpha_y < 1$, $T_x > 0$, and $T_y > 0$ are nonlinear gains associated with rapid convergence.

According to the transient and steady-state segmented convergence in [21], it is seen that the $\frac{1}{\alpha_\xi T_\xi}e^{|\cdot|^{-\alpha_\xi}}\mathrm{sig}(\cdot)^{1-\alpha_\xi}$ nonlinear term plays a central role in achieving rapid convergence within a predefined time. In contrast, the linear term ensures steady-state accuracy and accelerates transient convergence.

The stability of the control in the close-range docking phase is ensured by designing the following Lyapunov function

$$V_n = |e_{nx}| + |e_{ny}|, \quad (28)$$

and its derivative can meet as follows

$$\begin{aligned} \dot{V}_n \leq & -\frac{1}{\alpha_x T_x}e^{|e_{nx}|^{-\alpha_x}}|e_{nx}|^{1-\alpha_x} \\ & -\frac{1}{\alpha_y T_y}e^{|e_{ny}|^{-\alpha_y}}|e_{ny}|^{1-\alpha_y} \end{aligned} \quad (29)$$

It can be inferred from (28) and (29) that the control system in the close-range phase satisfies the stability conditions for rapid convergence in [21].

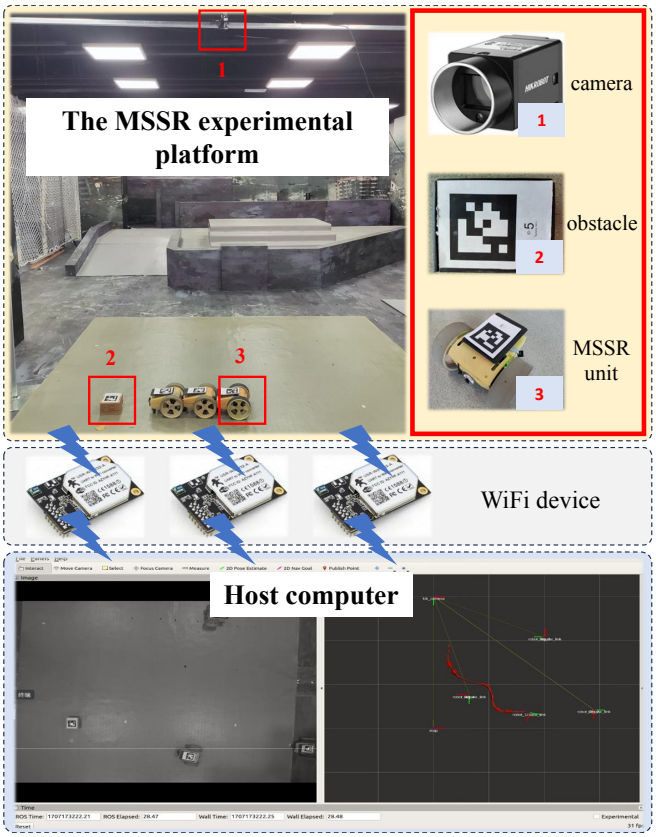

Fig. 5: Experimental Platform

V. Experimental Verification

A. Experimental Setup

The MSRR experimental platform is shown in Fig. 5. Each MSRR unit utilizes differential drive wheels for forward

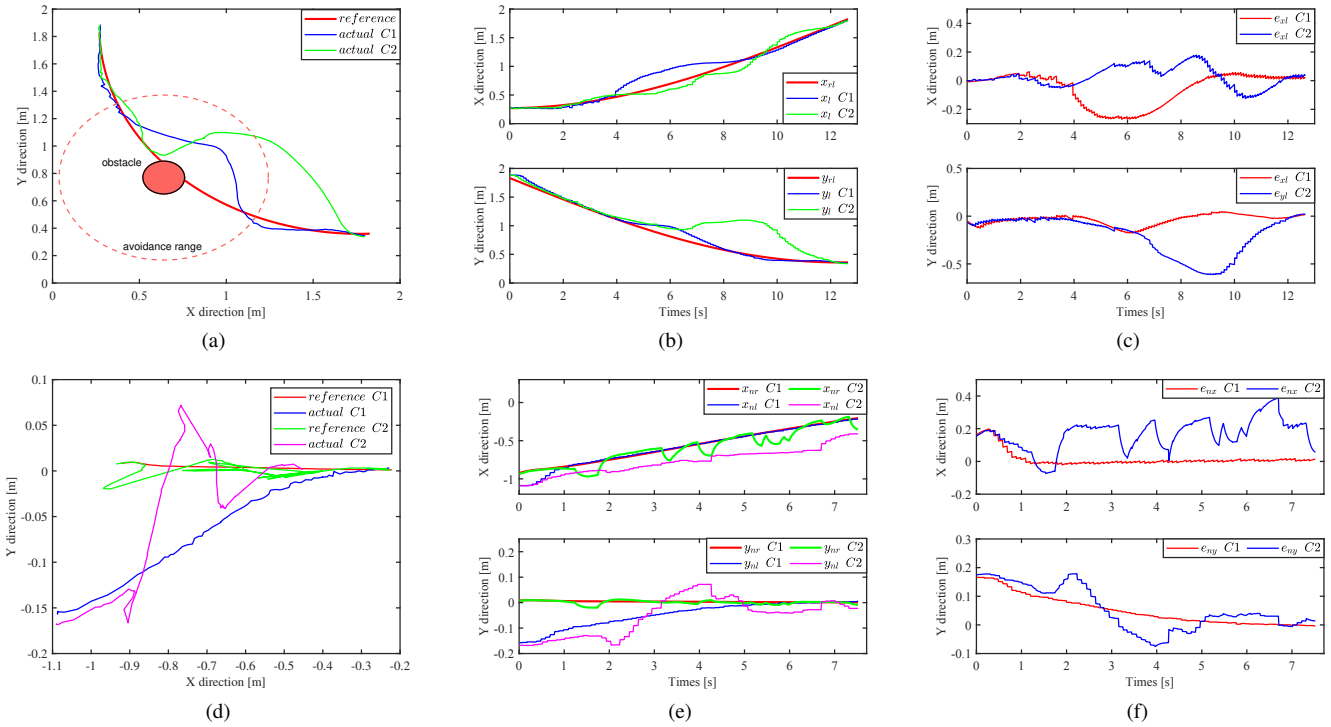

Fig. 6: The comparative results of the MSRR docking control. (a)–(c): the planar trajectory, trajectory tracking, and tracking errors in the long-distance phase. (d)–(f): the planar trajectory, trajectory tracking, and tracking errors in the close-range phase.

movement and steering actions. The position and orientation of each unit are acquired and identified through an overhead camera capturing Apriltags. Utilizing WiFi modules and router, a local communication network is established between the upper computer and each unit, enabling information sharing among units and real-time status monitoring and motion control by the host computer. In this section, the proposed control method and the obstacle avoidance and control method proposed in [22] are deployed in the long-distance and close-range control of the MSRR, respectively, denoted as C1 and C2, to compare and validate the application advantages of the proposed method in complex scenarios.

1) Long-distance phase: A circular trajectory is designed based on the global poses of the mobile unit and the docked unit, guiding the mobile unit to move to the position directly in front of the docked unit. Simultaneously, an obstacle $p_o = [x_o, y_o]^{\mathrm{T}}$ is placed on the desired trajectory as shown in Fig. 5 to verify the safety and smoothness of the proposed assembly trajectory tracking method. The positions of the obstacles can be obtained in real-time through the host computer by recognizing and calculating the Tags placed on top using a camera. The safe avoidance distance and the trigger distance, ρ_{sr} and ρ_{sR}, are 0.2 m and 0.65 m, respectively. The obstacle avoidance method proposed in [22] is compared with the proposed method to evaluate the effectiveness of safeness and smoothness. To ensure a fair comparison between the two methods, and through multiple practical parameter adjustments to obtain the optimal state for both methods.

2) Close-range phase: A straight-line guiding trajectory is designed based on the target for the docked unit. The mobile unit precisely moves to the docked target position by tracking the guiding trajectory using feedback from local perception. In this section, simulated local perception feedback of pose and LOS is constructed based on the global poses and coordinate transformations of the mobile and docked units. Guided trajectory tracking controllers are designed based on the proposed method and tracking method in [22]. In the comparison controllers, line-of-sight safety constraints are introduced in C1 and C2, but adaptive anti-windup is not included in C2. Similarly, both controllers utilize the same linear control gains.

B. Experimental Control Results

1) Long-distance phase: The proposed method is based on the dominant role of the upper-level avoidance guidance trajectory from nested windups and safety acceleration envelopes. It ensures complete safety near obstacles through the bottom-level virtual spring mechanism. Compared to the avoidance method in C2, the proposed safety mechanism exhibits obvious advantages in smoothness against nested windups. Figs. 6(b)–(c) reflect the transient response and steady-state accuracy of the two methods in assembling trajectories. In terms of tracking accuracy, the proposed method

(C1: $0.029\ \mathrm{m}$) is basically consistent with the comparative method (C2: $0.031\ \mathrm{m}$). However, its oscillation amplitude and recovery time for avoiding obstacles are $0.3\ \mathrm{m}$ and $3\ \mathrm{s}$, respectively, showing smoother characteristics compared to C2's oscillation amplitude and recovery time ($0.5\ \mathrm{m}$ and $6\ \mathrm{s}$). Fig. 6(a) depicts the plane of the docking and assembling process at the long-distance phase. The actual tracking trajectory of C1 is shorter and smoother than C2's avoidance journey, making it more suitable for complex docking scenarios with multiple obstacle distributions.

2) Close-range phase: Fig. 6(e) illustrates the trajectory tracking performance during the docking guidance process. At the initial stage, position errors trigger sudden changes in attitude, activating the LOS safety mechanism to adjust the reference trajectory to ensure that the mobile unit remains within the safe LOS. The combined linear and nonlinear control strategy facilitates precise and rapid convergence of the docking trajectory to the guidance trajectory, ensuring the insertion of the locking device into the location hole, as demonstrated by Fig. 6(d) for C1, which exhibits smoothness and safety during the docking process. However, C2, without the induction of adaptive windup, is prone to oscillate when the LOS safety mechanism is triggered. In Figs. 6(d)–(e), the trajectory of the mobile unit becomes uncontrolled. It exhibits severe oscillations, leading to frequent corrections of the guidance trajectory and ultimately preventing the successful completion of close-range docking. Fig. 6(f) depicts the tracking errors of the docking guidance trajectory in the close-range stage. With a docking accuracy requirement of $0.015\ \mathrm{m}$, C1 reaches the range of docking accuracy in 4 seconds, with a final control accuracy of $0.007\ \mathrm{m}$. In contrast, C2 is uncontrollable, with a final control accuracy of $0.044\ \mathrm{m}$.

VI. Conclusions

For the practical requirements and limitations of existing methods for mobile self-reconfigurable robot systems in engineering applications, the paper proposes a segmented secure docking control framework based on global localization and local perception. The framework aims to address challenges such as differences in sensor perception characteristics, obstacles' safety threats, and motion performance constraints. Firstly, in the remote distance phase, a dual-layer constraint control framework of upper-level obstacle avoidance guidance and lower-level trajectory tracking is proposed to achieve the safe assembly of reconfigurable units. Secondly, in the close distance phase, active line-of-sight correction and adaptive windup control are integrated to achieve rapid tracking of straight-line guidance trajectories and precise docking within the LOS range. Finally, the effectiveness of the proposed method is verified through comparative physical experiments.

References

[1] C. Liu, M. Whitzer, and M. Yim, "A distributed reconfiguration planning algorithm for modular robots," *IEEE Robotics and Automation Letters*, vol. 4, no. 4, pp. 4231–4238, 2019.

[2] W. Cheah, B. V. Adorno, S. Watson, et al., "Set-point control for a ground-based reconfigurable robot," in *Proc. 2022 IEEE/RSJ International Conference on Intelligent Robots and Systems (IROS)*, pp. 2616–2621, 2022.

[3] S. M. B. P. Samarakoon, M. A. V. J. Muthugala, A. V. Le, et al., "Toward complete area coverage of a reconfigurable tiling robot by following obstacle shape," *Complex and Intelligent Systems*, vol. 7, no. 2, pp. 741–751, 2021.

[4] S. S. Sohal, B. Sebastian, and P. Ben-Tzvi, "Autonomous docking of hybrid-wheeled modular robots with an integrated active genderless docking mechanism," *Journal of Mechanisms and Robotics*, vol. 14, no. 1, pp. 011010, 2022.

[5] C. Park, J. Bae, S. Ryu, J. Lee, and T. Seo, "R-track: Separable modular climbing robot design for wall-to-wall transition," *IEEE Robotics and Automation Letters*, vol. 6, no. 2, pp. 1036–1042, 2020.

[6] B. Huang, B. Zhou, H. Pang, X. Jian, and H. Fang, "A reliable docking mechanism and close-range docking algorithm for modular reconfigurable robots," in *Proc. 2023 9th International Conference on Mechatronics and Robotics Engineering (ICMRE)*, pp. 78–83, 2023.

[7] W. Tan, H. Wei, and B. Yang, "SambotII: a new self-assembly modular robot platform based on sambot," *Applied Sciences*, vol. 8, no. 10, 1719, 2018.

[8] H. Li, H. Wang, L. Cui, J. Li, and Q. Wei, "Design and experiments of a compact self-assembling mobile modular robot with joint actuation and onboard visual-based perception," *Applied Sciences*, vol. 12, no. 6, 3050, 2022.

[9] Y. Quiñonez, J. Baca, J. de Lope, and R. Aracil, "Self-alignment approach based on cooperative behaviors for the docking process of modular mobile robots," in *Proc. 2010 IEEE Electronics, Robotics and Automotive Mechanics Conference*, pp. 445–450, 2010.

[10] H. Wei, Y. Chen, and J. Tan, "Sambot: A self-assembly modular robot system," *IEEE/ASME Transactions on Mechatronics*, vol. 16, no. 4, pp. 745–757, 2010.

[11] H. X. Wei, H. Y. Li, and Y. Guan, "A dynamics based two-stage path model for the docking navigation of a self-assembly modular robot (Sambot)," *Robotica*, vol. 34, no. 7, pp. 1517–1528, 2016.

[12] C. Liu, Q. Lin, H. Kim, and M. Yin, "SMORES-EP, a modular robot with parallel self-assembly," *Autonomous Robots*, vol. 47, no. 2, pp. 211–228, 2023.

[13] W. Zhang, W. Wu, and Y. Teng, "An underwater docking system based on UUV and recovery mother ship: design and experiment," *Ocean Engineering*, vol. 281, 114767, 2023.

[14] Y. Zhang, P. Huang, K. Song, and Z. Meng, "An Angles-Only Navigation and Control Scheme for Noncooperative Rendezvous Operations," *IEEE Transactions on Industrial Electronics*, vol. 66, no. 11, pp. 8618–8627, Nov. 2019.

[15] S. Chang, Y. Wang, Z. Zuo, and H. Yang, "Fixed-time formation control for wheeled mobile robots with prescribed performance," *IEEE Transactions on Control Systems Technology*, vol. 30, no. 2, pp. 844–851, 2021.

[16] G. Xia, X. Xia, and Z. Zheng, "Formation tracking control for underactuated surface vehicles with actuator magnitude and rate saturations," *Ocean Engineering*, vol. 260, 111935, 2022.

[17] A. Ghaffari, "Analytical design and experimental verification of geofencing control for aerial applications," *IEEE/ASME Transactions on Mechatronics*, vol. 26, no. 2, pp. 1106–1117, 2020.

[18] M. Ran, J. Li, and L. Xie, "A new extended state observer for uncertain nonlinear systems," *Automatica*, vol. 131, 109772, 2021.

[19] F. Huang, X. Chen, Z. Chen, and Y. Pan., "A novel SMMS teleoperation control framework for multiple mobile agents with obstacles avoidance by leader selection," *IEEE Transactions on Systems, Man, and Cybernetics: Systems*, vol. 53, no. 3, pp. 1517–1529, 2022.

[20] K. Zhao, J. Zhang, and D. Ma, "Composite disturbance rejection attitude control for quadrotor with unknown disturbance," *IEEE Transactions on Industrial Electronics*, vol. 67, no. 8, pp. 6894–6903, 2019.

[21] S. Huang, L. Xiong, and Y. Zhou, "A novel distributed predefined-time sliding mode controller for performance enhancement of power system under input saturation," *IEEE Transactions on Circuits and Systems I: Regular Papers*, vol. 69, no. 10, pp. 4284–4297, 2022.

[22] R. S. Sharma, A. Mondal, and L. Behera, "Tracking control of mobile robots in formation in the presence of disturbances," *IEEE Transactions on Industrial Informatics*, vol. 17, no. 1, pp. 110–123, 2020.